Available online at www.sciencedirect.com

ScienceDirect

Nuclear Physics A 994 (2020) 121665

NUCLEAR PHYSICS A

www.elsevier.com/locate/nuclphysa

Role of the dynamical polarization potential in explaining the $\alpha + {}^{12}C$ system at low energies

Y. Kucuk [a,*], A. Soylu [b], L.C. Chamon [c]

[a] *Department of Physics, Akdeniz University, Antalya, Turkey*
[b] *Department of Physics, Niğde Ömer Halisdemir University, 51240, Niğde, Turkey*
[c] *Depto. de Física Nuclear, Sao Paulo University, Sao Paulo, SP, Brazil*

Received 7 July 2019; received in revised form 23 October 2019; accepted 4 November 2019
Available online 9 November 2019

Abstract

In this paper, we have analyzed the elastic scattering data of the $\alpha + {}^{12}C$ system at 13, 18, 54.1 and 60 MeV incident energies within the framework of the double folding model. We have modified the shape of the real and imaginary parts of the optical potential simultaneously, in the surface region, in order to take into account the effects of the dynamical polarization. With this, we have been able to obtain an improved agreement of the theoretical cross sections with the experimental data. We have also calculated α-cluster states in ^{16}O using the same potential. We have shown that the inclusion of the dynamical polarization potential (DPP) in the bare folding potential provides an improvement also in producing the ^{16}O rotational bands and corresponding excitation energies. Thus, DPP effect is important in explaining the reaction observables of $\alpha + {}^{12}C$ system as well as the structure of the ^{16}O at low energies

Keywords: Elastic scattering; Dynamical polarization potential; Double folding potential

1. Introduction

Reactions induced by α particle take enormous interest since they play a major role in stellar nucleosynthesis. The elastic and inelastic scattering of ^{4}He on light nuclei have been studied in

* Corresponding author.
E-mail address: ykucuk@akdeniz.edu.tr (Y. Kucuk).

https://doi.org/10.1016/j.nuclphysa.2019.121665
0375-9474/

a wide energy range during several decades [1–7], and cross section data have been measured to understand the reaction mechanism of alpha-nucleus systems. Alpha-particle scattering is also important to study the alpha cluster structure of light nuclei [8,9]. Many experiments have been conducted to explore the structure and to survey the cluster models. As parallel to the experimental studies, many theoretical analysis have been made within several approaches to interpret the behavior of the data, as well as the phenomenons observed in α-nucleus systems such as the anomalous large-angle scattering (ALAS) [1–7]. One of these systems is ^{4}He+^{12}C, which has been extensively studied for both low and high energy regions. While standard reaction models such as the Optical Model (OM) could explain the high energy data very well, the experimental elastic scattering cross sections at low energies could not be properly described using these models without taking into account the effects of couplings [10,11]. Recent paper by Chamon et al. [12] discussed the significance of the couplings to excited states for the elastic scattering of this system at low energies ($E_{Lab} \leqslant 10.5$ MeV). They analyzed the integrated inelastic cross section for the 2^{+} ^{12}C state, the capture process ^{4}He + ^{12}C $\rightarrow$ p + ^{15}N, and phase-shifts that describe the experimental elastic scattering cross sections. They have shown that the effect of couplings to inelastic states are important for the elastic scattering and capture reaction processes at low energies. They also showed that the corresponding polarization potential presents a quite complicate behavior as a function of angular momentum and energy.

Recently, many studies have also been performed in order to search for an alpha-cluster structure of the ^{16}O [13–20]. The nuclear properties of ^{16}O have been investigated using the binary cluster model, in which it is considered as an $\alpha + ^{12}$C cluster-core system [21]. The energies and widths for the states of two ^{16}O rotational bands have been obtained through the potential model [22]. Katsuma has investigated the unknown 8^{+} and 9^{-} states for rotational bands of ^{16}O, by using an OM potential of $\alpha + ^{12}$C elastic scattering data in $E_{c.m.}$= 21.15 to 26.625 MeV [23,24]. In this study, he showed that the 0^{+} state has the total quantum number N = 8 of the $\alpha + ^{12}$C rotational bands [23,24]. The elastic and inelastic $\alpha + ^{12}$C scattering and the states with the $\alpha + ^{12}$C cluster have been analyzed using the double folding model in the coupled channel method, by taking into account the excited states of the ^{12}C nucleus [25].

In the present paper, we are motivated to analyze some low and intermediate energy data which have not been studied in detail, and to understand the behavior of the dynamical polarization potential (DPP), which takes into account the non-elastic channels for the ^{4}He+^{12}C system. With this purpose, we have chosen four different incident energies of the α-particle, 13.0, 18.0, 54.1 and 60.0 MeV. We have analyzed the elastic scattering cross sections within the framework of the double folding model. We also use the model to study properties of the $\alpha + ^{12}$C cluster structure of the ^{16}O nucleus. The next section describes the model used in the calculations. The results and discussions are found in the following sections.

2. Model

Fig. 1 shows the experimental elastic scattering angular distributions (ratio to Rutherford) for $\alpha + ^{12}$C that we analyze in the present work. The data were obtained in [4]. Before proceeding with the data fits, we first compare the data set with standard results obtained with the São Paulo potential (SPP). The SPP is a model for the real part of the optical potential (OP) that involves an extensive systematics for the nuclear densities [26]. It has been adopted in many data analyzes for elastic scattering and fusion of several heavy-ion systems. In [27], a phenomenological extension of the model to the imaginary part of the OP was proposed. The imaginary part was found to be proportional to the real one, with a factor of normalization about 0.8. With this, the

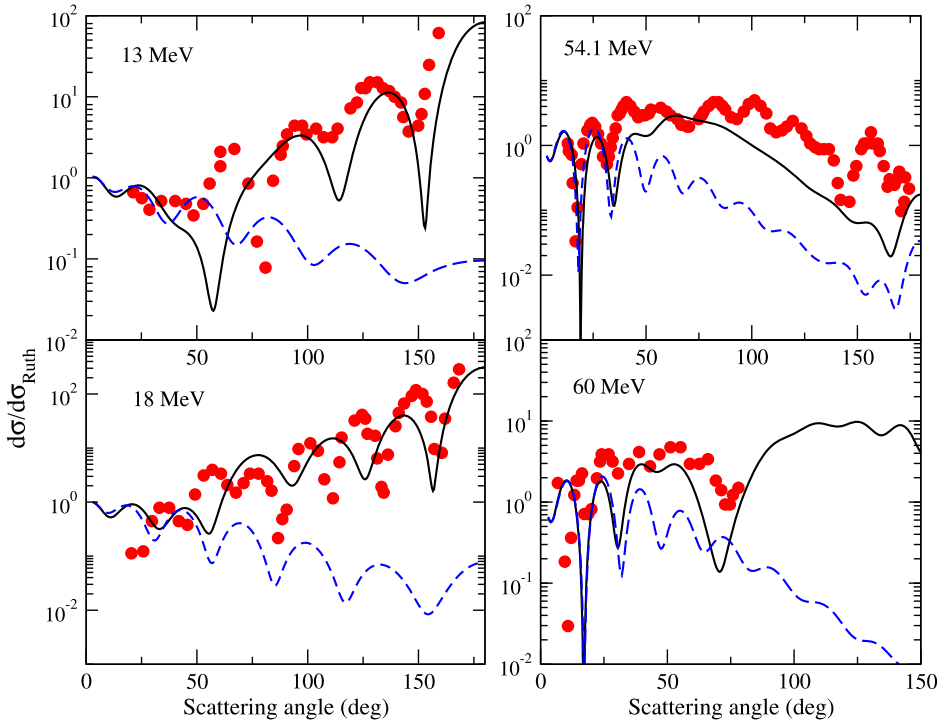

Fig. 1. Experimental elastic scattering angular distributions for $\alpha + {}^{12}C$ obtained from [4]. The dashed lines represent results obtained with the SPP, while the solid lines correspond to the OM data fits obtained in the context of the bare folding potential.

model does not contain any adjustable parameter and has accounted for the description of many elastic scattering data sets for several systems (see e.g. [27]). The dashed blue lines in Fig. 1 represent the results obtained with the SPP in the cases considered in the present work. Clearly, the data present a behavior quite different in comparison with the standard theoretical predictions obtained with the parameter-free SPP.

From now on, we assume the real and imaginary parts of the OP as:

$$U(R) = N_R\, V_{DF}(R) + i\, \frac{W_0}{1 + \exp[(R - R_W)/a_W]}, \tag{1}$$

where $V_{DF}(R)$ is determined within the framework of the double folding model. The potential is evaluated by folding the nuclear matter distributions with the effective nucleon-nucleon interaction (v_{nn}):

$$V_{DF}(R) = \int d\vec{r}_1 \int d\vec{r}_2\, \rho_p(\vec{r}_1)\, \rho_t(\vec{r}_2)\, v_{NN}(\vec{r}_{12}), \tag{2}$$

where $\rho_P(\vec{r}_1)$ and $\rho_T(\vec{r}_2)$ are the nuclear matter densities of the projectile and target nuclei, $\vec{r}_{12} = \vec{R} - \vec{r}_1 + \vec{r}_2$ and N_R is the normalization factor.

The nuclear matter density distribution for ^{12}C has been assumed as a two-parameter Fermi function:

$$\rho_T(r_1) = \frac{\rho_0}{1 + exp(\frac{r_1 - a}{c})}, \tag{3}$$

Table 1
Values of the parameters of the real and imaginary parts of the OP of the standard double folding calculations and the volume integrals of the potentials.

E_{Lab} MeV	N_V	W_0 MeV	r_W fm	a_W fm	J_V MeV fm^3	J_W MeV fm^3
13.0	0.88	2.5	1.1	0.9	367	23
18.0	0.93	3.0	0.8	0.94	386	14
54.1	1.0	18.0	0.8	0.94	402	86
60.0	0.55	17.0	0.8	0.94	220	81

where the parameters ρ_0, a and c have been chosen to reproduce the rms matter radius of ^{12}C [28]. For the alpha particle, the density distribution has been taken from [29].

We have chosen the M3Y realistic interaction for the effective nucleon-nucleon interaction:

$$v_{NN}(r) = 7999\frac{e^{-4r}}{4r} - 2134\frac{e^{-2.5r}}{2.5r} + J_{00}(E)\,\delta(\vec{r}), \tag{4}$$

where $J_{00}(E)$ represents the exchange term, since nucleon exchange is possible between projectile and target. $J_{00}(E)$ has a linear energy-dependence and is expressed as

$$J_{00}(E) = 276\,[1 - 0.005\,E/A_P]\,(\text{MeV}). \tag{5}$$

While the real part of the OM has been obtained by using the above-described model, the imaginary potential has been taken in Woods-Saxon form, according to Equation (1), where $R_W = r_W\,(A_P^{1/3} + A_T^{1/3})$, A_P and A_T are the mass numbers of projectile and target nuclei. In our calculations, the value of the diffuseness parameter a_W has been taken around to 0.9 fm, in order to reduce the number of free parameters. The depth W_0 and radius of the imaginary potential, as well as the normalization factor N_R of the real part of the OP, have been adjusted to fit the experimental data. The parameter values obtained in these calculations are presented in Table 1. In this table we present also the volume integrals of the real and imaginary potentials calculated by using the following formula:

$$J_{V,W}(E) = \frac{-4\pi}{A_P + A_T}\int V, W(r, E)\, r^2\, dr. \tag{6}$$

The OP presents an energy dependence in scattering of strongly bound nuclei. When the bombarding energy approaches the Coulomb barrier, the strength of the imaginary potential decreases because the reaction channels close down at energies below the Coulomb barrier. On the other hand, the real part of the OP varies sharply. This behavior is named as threshold anomaly, and it is due to the effects of the coupling to the non-elastic channels. The couplings produce the dispersion relation which connects the real and imaginary parts of the OP. The dispersion relation is a general concept in physics and is a consequence of the causality principle. It is given by:

$$\begin{aligned} ReU(E, R, R') &= V_0(R) + \sum_n \frac{A_n(R, R')}{E - E_n} + \frac{P}{\pi}\int_{\epsilon_n}^{\infty} \frac{ImU(E', R, R')}{E' - E} dE' \\ &= V_0(R) + \Delta V(E, R) \end{aligned} \tag{7}$$

where P denotes the principal value [30,31]. The term $\Delta V(E, R)$ is called Dynamic Polarization Potential (DPP). It is necessary to take account the DPP in the OP since the coupling effects are not included in the bare potential [30]. One way to include the DPP in the one-body volume

Table 2
Values of the parameters of the real and imaginary parts of the Dynamical Polarization Potential.

E_{Lab} MeV	V_0 MeV	r_V fm	a_V fm	W_0 MeV	r_W fm	a_W fm	J_V MeV fm^3	J_W MeV fm^3
13.0	-7.9	0.8	0.94	-1.	0.8	0.94	-90	-11
18.0	9.0	1.35	0.99	1.0	0.8	0.94	201	11
54.1	13.0	0.8	0.69	1.0	0.8	0.94	104	11
60.0	20.0	0.95	0.65	1.0	0.8	0.94	202	11

potential is to add a surface potential with the shape of a Woods-Saxon derivative, as done in Refs. [32] and [33]. In the present work, we have used the same methodology and modified the shape of the real and imaginary parts of the folding potential by adding two small potentials to these parts at the surface region to take into account of the coupling effects at low energies. We show the DPP parameter values as well as the volume integrals in Table 2.

3. Results and discussion

We have analyzed the elastic scattering angular distributions of ^{4}He +^{12}C at four energies through the OM. Since phenomenological potentials are not adequate to explain the elastic scattering cross sections at low energies, we have assumed the double folding potential, which is a more realistic model for the real part of the OP, with the Woods-Saxon shaped imaginary potential to examine the data. We kept the radius and diffuseness parameters of the imaginary part as constant values for 18.0, 54.1 and 60.0 MeV (see Table 1). For 13 MeV, these parameter values have been changed to 1.1 and 0.9, to obtain a better agreement of the theoretical cross sections with the data. As shown in Table 1, although N_R and W_0 have been varied depending on the energy, the double folding potential could not produce a good agreement of the theoretical cross sections (solid black lines in Fig. 1) with the experimental data at low and intermediate energies. The failure of the standard double folding potential and of the SPP in accounting for the data shows that the inclusion of the coupling to non-elastic channels is necessary at these energies, as has also been observed at lower energies [12]. These effects are not included in the bare OP, has been taken into account with an additional potential to include DPP effect. The modified folding model provides an improvement in explaining the low and intermediate energy data, as shown in Fig. 2. We assumed the adjusted parameter values of the imaginary part of the DPP as identical for all energies, while the parameters of the real part were varied depending on energy to obtain the best data fit. We point out that similar procedure of modification of the SPP by additional DPP potentials in the surface region could not provide a good agreement between data and theoretical cross sections. Since the SPP involves a different effective nucleon-nucleon interaction instead of the M3Y interaction, which has been used in the standard folding model, a different methodology could be required instead of the phenomenological DPP assumed in this work. On the other hand, we verified that the agreement between the theoretical calculations and data can be improved in the context of the SPP if an internal and very deep imaginary potential is assumed for the OP, instead of the standard imaginary part proportional to the real one (with factor of normalization of 0.8).

Usually, the DPP is an attractive potential. However, it has been observed that DPP is repulsive in interactions involving weakly-bound nuclei [34]. In our calculations for ^{4}He + ^{12}C, we have also observed that the character of DPP changes depending on the energy. As shown in Fig. 3, we have studied the effect of DPP when it is repulsive and attractive. For this purpose, we have

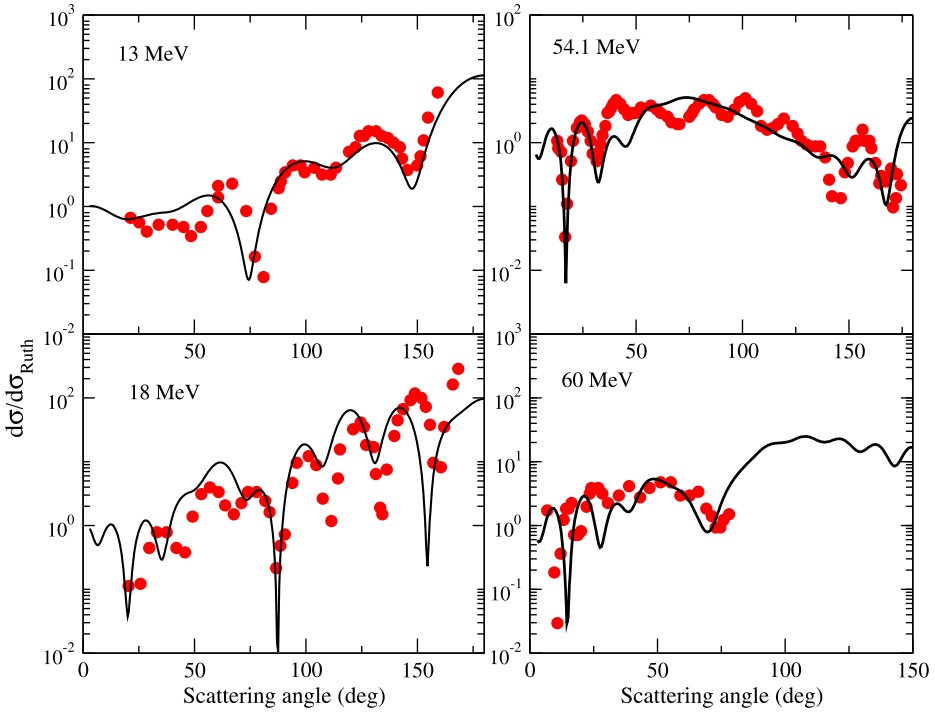

Fig. 2. Elastic scattering angular distributions at 13, 18, 54.1 and 60.0 MeV. The solid lines represent OM results obtained with the folding potential with the DPP effect (see text for details).

searched for a potential that produces the best fit for the two cases: the attractive and repulsive DPP separately. As shown in Fig. 3, the repulsive DPP produces better agreement at 13 MeV, while the attractive DPP produces better agreement at 18 MeV. To avoid confusion, in Table 2 we have shown only the potential sets that provide the best data fits. As seen from this table, DPP must be repulsive at 13 MeV while it must be attractive at 18, 54.1 and 60 MeV 3.

We have also shown volume integrals and dispersion relation (DR) between real and imaginary parts of the modified potential in Fig. 4. The imaginary part of the OP volume integral (of the four energies) follows the usual behavior of the threshold anomaly, as illustrated by solid lines in Fig. 4. The corresponding real part of the DR has been calculated by

$$J_V(E) = V_R - \frac{W}{\pi}[\epsilon_a \ln|\epsilon_a| - \epsilon_b \ln|\epsilon_b|]. \tag{8}$$

Here $\epsilon_i = (E - E_i)/(E_b - E_a)$ with i as a and b respectively [30,31]. The parameters are $E_a =$ 5 MeV, $E_b = 50.0$ MeV, $V_R = 500$ MeV and $W = 100$ MeV. As seen in the figure, the real part of the modified potential is in reasonable agreement at 18, 54.1 and 60 MeV, except in the case of the lowest energy at 13 MeV because of the positive sign of DPP at this energy. This behavior might be related to some resonance near this energy, maybe related to a term like $\frac{A_n(R,R')}{E-E_n}$ in Equation (7).

We have also used the same modified folding potential, bare plus DPP, to obtain the energies of resonant states of ^{16}O with the Gamow code [35]. Gamow code is used to calculate the resonant state solution of the radial Schrödinger equation for an arbitrary optical potential. In this study,

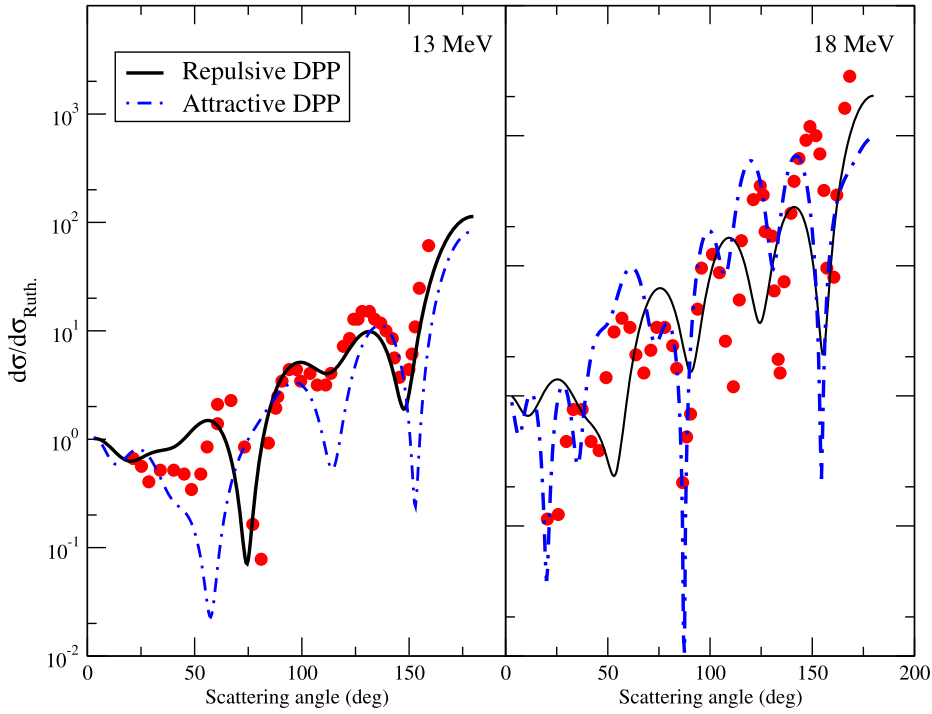

Fig. 3. The effect of repulsive and attractive DPP at 13 and 18 MeV.

it was used to calculate excitation energies of cluster states of ^{16}O with the corresponding global quantum number G. When one considers $\alpha + {}^{12}$C for ^{16}O, the problem is converted to two-body and then the cluster states of ^{16}O can be calculated by using global quantum number. The global quantum number G comes from the Wildermuth rule [36], which represents the effect of the Pauli principle by allowing cluster nucleons to occupy low-lying orbital. It is given by $G = 2n + L = \sum_{j=1}^{n_c} 2n_j + l_j$, where n_c is the number of cluster nucleons, n_j and l_j are the single particle quantum numbers. The minimum value of G, allowed by the Pauli principle, can be obtained in the spherical shell model. In this prescription, G = 8 and 9 are used for ^{16}O.

To make a comparison, the calculations have been performed considering two cases: assuming only the bare double folding approach (DF) and with bare plus DPP potentials. The same potential that reproduced the experimental elastic scattering angular distributions was used to obtain the cluster states in ^{16}O using the GAMOW code. However, given the nature of the potential, naturally this procedure does not reproduce exactly the experimental excitation energies of the states. Hence, as a further step, we found out the normalization parameter N_R values of the potential that provide the known experimental excitation energy of the 4^+ state to constrain the potential. Therefore, this was fixed in the calculations. In fact this changed only the depth of the interaction potential. Experimental excitation energies and decay widths values are taken from Refs. [37] and [38]. Correspondingly, we have used the following N_R values: 0.937 for DF potential, 0.810 for DF+DPP potential at 13 MeV, 0.942 for DF potential at 18 MeV, 0.806 for DF+DPP potential at 54 MeV, 0.657 for DF+DPP potential at 60 MeV.

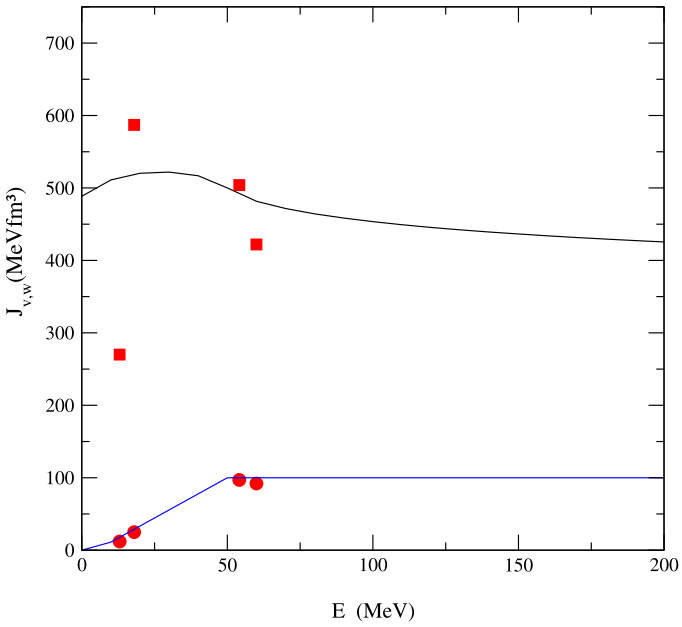

Fig. 4. Volume integrals of the real and imaginary parts of the modified folding potential. Here squares show the real potential and circles show the imaginary potentials. Dispersion relation of the potentials has been calculated by Equation (8).

Table 3
Resonant state energies for ^{16}O calculated with DF and DF+DPP potentials that were obtained from elastic scattering data fits at $E_{Lab} = 13$ and 18 MeV. Experimental values are taken from Refs. [37] and [38]. – means that experimental values do not exist for these energies, while – – – means that a reasonable value could not be obtained for the particular states.

					$E_x - i\Gamma/2$	
St.	G	E_x [MeV]	Γ_α^{exp} [keV]	13 MeV (DF)	13 MeV (DF+DPP)	18 MeV (DF)
0^+	8	–	–	5.341-0.000	5.789-0.000	5.344-0.000
2^+	8	–	–	– – –	7.022-0.000	– – –
4^+	8	10.35	27 ± 4	10.350-0.154	10.350-0.336	10.349-0.157
6^+	8	16.27	392 ± 20	15.993-0.177	15.306-0.280	12.384-0.973
8^+	8	–	–	14.803-1.016	18.462-1.780	14.794-0.998
1^-	9	9.63	400 ± 10	– – –	– – –	– – –
3^-	9	11.6	800 ± 100	– – –	– – –	– – –
5^-	9	14.66	632 ± 20	10.248-0.310	17.360-1.051	– – –
7^-	9	20.86	540 ± 100	– – –	– – –	10.248-0.312
9^-	9	–	–	– – –	30.802 -0.564	– – –

In Tables 3 and 4, we present excitation energy results obtained with the DF and DF + DPP potentials. In these Tables, $E_x = E + E_{thr.}$, with $E_{thr.} = 7.162$ MeV. In Figs. 5 and 6, we plot the ^{16}O excitation energies as a function of $J(J+1)$ for G = 8, positive parity states, using the potentials that fit the data at 13 MeV and 60 MeV, respectively. It should be noted that the bare

Table 4
The same as Table 3, but with potentials obtained with potentials from the elastic scattering data fits for $E_{Lab} = 54.1$ and 60 MeV.

				$E_x - i\Gamma/2$		
St.	G	E_x [MeV]	Γ_α^{exp} [keV]	54 MeV (DF)	54 MeV (DF+DPP)	60 MeV (DF+DPP)
0^+	8	–	–	5.323-0.000	– – –	7.394-0.000
2^+	8	–	–	– – –	7.448-0.000	8.273-0.003
4^+	8	10.35	27 ± 4	10.350-0.303	10.350-0.567	10.350-0.564
6^+	8	16.27	392 ± 20	12.339-0.628	15.056-0.176	– – –
8^+	8	–	–	14.965-0.765	15.242-0.921	18.407-0.177
1^-	9	9.63	400 ± 10	– – –	– – –	12.700-1.037
3^-	9	11.6	800 ± 100	– – –	– – –	13.682-1.259
5^-	9	14.66	632 ± 20	10.305-0.435	17.452-0.696	17.972-0.893
7^-	9	20.86	540 ± 100	– – –	13.921-0.772	21.039-0.672
9^-	9	–	–	16.368-0.948	16.595-1.131	16.783-1.211

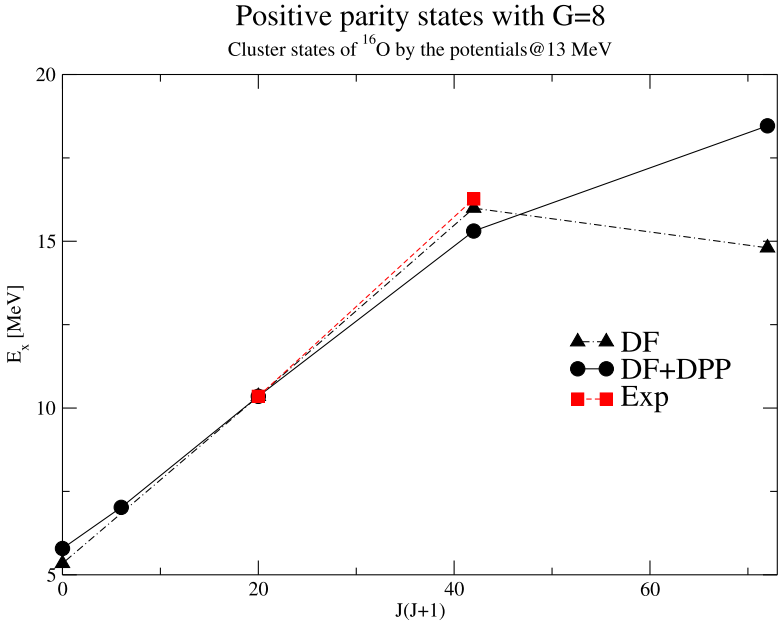

Fig. 5. Excitation energies for ^{16}O versus $J(J+1)$ for G=8, positive parity states for the DF and DF+DPP potentials at 13 MeV.

DF potential does not produce the energies of resonant states of ^{16}O at 60 MeV. As seen in these figures, the DPP has significant effect also in producing the cluster states of ^{16}O.

4. Summary

In this paper, we have analyzed α + ^{12}C elastic scattering data in the framework of the OM, using a realistic double folding potential for the real part of the OP and the Woods-Saxon shape for the imaginary part. Since this folding potential was not adequate to explain the experimental

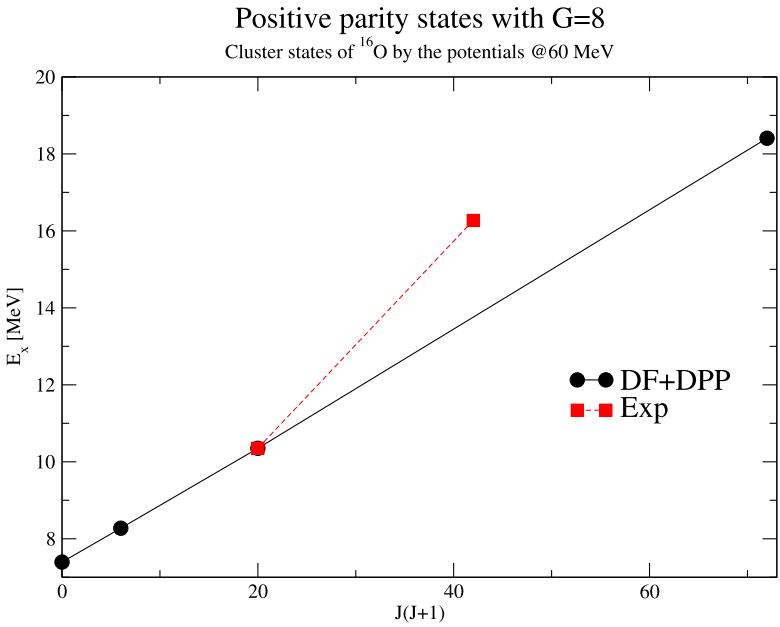

Fig. 6. Excitation energies for ^{16}O versus $J(J+1)$ for G=8, positive parity states for DF+DPP potentials at 60 MeV. Bare DF potential does not produce resonant energies at 60 MeV.

angular distributions and also the rotational bands of ^{16}O, we have modified the bare folding potential to include the DPP effect. DPP has provided a better agreement of theoretical results with the experimental data of cross sections and rotational bands simultaneously at low and intermediate energies. We have shown the role of DPP in describing the reaction observables and structure properties at the same time. We have also shown that the character of DPP changes depending on energy for the $\alpha + {}^{12}$C system.

Acknowledgements

This work was supported by Scientific Research Project Coordination Unit of Akdeniz University. Project number: 3518.

References

[1] N. Baron, R.F. Leonard, W.M. Stewart, Phys. Rev. C 4 (1971) 1159.
[2] H. Oeschler, H. Fuchs, H. Schröter, Nucl. Phys. A 202 (1973) 513–529.
[3] M. Yasue, T. Tanabe, F. Soga, J. Kokame, F. Shimokoshi, J. Kasagi, Y. Toba, Y. Kadota, T. Ohsawa, K. Furuno, Nucl. Phys. A 394 (1983) 29–38.
[4] R.F. Lichtenthäler, A.C.C. Villari, A. Lépine-Szily, L.C. Gomes, Phys. Rev. C 44 (1991) 1152–1155.
[5] S.A.E. Khallaf, A.M.A. Amry, S.R. Mokhtar, Phys. Rev. C 56 (1997) 2093.
[6] D.T. Khoa, Phys. Rev. C 63 (2001) 034007.
[7] T.L. Belyaeva, A.N. Danilov, A.S. Demyanova, S.A. Goncharov, A.A. Ogloblin, R. Perez-Torres, Phys. Rev. C 82 (2010) 054618.
[8] S. Ohkubo, Y. Hirabayashi, Phys. Lett. B 684 (2010) 127–131.
[9] M. Freer, N.I. Ashwood, N.L. Achouri, W.N. Catford, N. Curtis, F. Delaunay, H. Al Faloub, F.M. Marqués, T. Munoz Britton, N.A. Orr, R. Raabe, N. Soíc, J.S. Thomas, V.A. Zimana, Phys. Lett. B 775 (2017) 58–62.

[10] E.B. Carter, G.E. Mitchel, R.H. Davis, Phys. Rev. 133 (1964) 1421–1433.
[11] Y.X. Yang, Q.R. Li, Nucl. Phys. A 732 (2004) 3–12.
[12] L.C. Chamon, L.R. Gasgues, L.F.M. Alves, V. Guimarães, P. Descouvemont, R.J. deBoer, M. Wiescher, J. Phys. G, Nucl. Part. Phys. 41 (2014) 035101.
[13] C.J. Halcrow, C. King, N.S. Manton, Phys. Rev. C 95 (2017) 031303.
[14] R. Bijker, F. Iachello, Nucl. Phys. A 957 (2017) 154–176.
[15] M. Freer, H. Horiuchi, Y. Kanada-Enyo, D. Lee, U.G. Meißner, Rev. Mod. Phys. 90 (3) (2018) 035004.
[16] A. Soylu, F. Koyuncu, A. Coban, O. Bayrak, M. Freer, Ann. Phys. 391 (2018) 263–277.
[17] T. Fukui, Y. Kanada-En'yo, K. Ogata, T. Suhara, Y. Taniguchi, Nucl. Phys. A 983 (2019) 38–52.
[18] Y. Funaki, T. Yamada, H. Horiuchi, G. Röpke, P. Schuck, A. Tohsaki, Prog. Theor. Phys. Suppl. 196 (2012) 439–444.
[19] Y. Funaki, A. Tohsaki, H. Horiuchi, P. Schuck, G. Röpke, Mod. Phys. Lett. A 21 (2006) 2331–2340.
[20] X.B. Wang, G.X. Dong, Z.C. Gao, Y.S. Chen, C.W. Shen, Phys. Lett. B 790 (2019) 498–501.
[21] B. Buck, C.B. Dover, J.P. Vary, Phys. Rev. C 11 (1975) 1803.
[22] B. Buck, J.A. Rubio, J. Phys. G, Nucl. Phys. 10.9 (1984) L209.
[23] M. Katsuma, J. Phys. G, Nucl. Part. Phys. 40 (2013) 025107.
[24] M. Katsuma, EPJ Web Conf. 66 (2014) 03041.
[25] S. Ohkubo, Y. Hirabayashi, Phys. Lett. B 684 (2010) 1271.
[26] L.C. Chamon, B.V. Carlson, L.R. Gasques, D. Pereira, C. De Conti, M.A.G. Alvarez, M.S. Hussein, M.A. Cândido Ribeiro, E.S. Rossi Jr., C.P. Silva, Phys. Rev. C 66 (2002) 014610.
[27] M.A.G. Alvarez, L.C. Chamon, M.S. Hussein, D. Pereira, L.R. Gasques, E.S. Rossi Jr., C.P. Silva, Nucl. Phys. A 723 (2003) 93.
[28] H. De Vries, C.W. De Jager, C. De Vries, At. Data Nucl. Data Tables 36 (1987) 495.
[29] G.R. Satchler, W.G. Love, Phys. Rep. 55 (1979) 183.
[30] G.R. Satchler, Phys. Rep. 199 (1991) 147.
[31] C. Mahauz, H. Ngo, G.R. Satchler, Nucl. Phys. A 449 (1986) 354–394.
[32] I. Boztosun, Phys. Rev. C 66 (2002) 1.
[33] A. Un, Y. Kucuk, T. Caner, I. Boztosun, Phys. Rev. C 89 (2014) 057605.
[34] M. Zadro, P. Figuera, A. Di Pietro, F. Amorini, M. Fisichella, O. Goryunov, M. Lattuada, C. Maiolino, A. Musumarra, V. Ostashko, M. Papa, M.G. Pellegriti, F. Rizzo, D. Santonocito, V. Scuderi, D. Torresi, Phys. Rev. C 80 (2009) 064610.
[35] T. Vertse, K. Pál, Z. Balogh, Comput. Phys. Commun. 27 (1982) 309.
[36] K. Wildermuth, Y.C. Tang, A Unified Theory of the Nucleus, Academic Press, New York, 1997.
[37] F. Ajzenberg-Selove, Nucl. Phys. A 375 (1982) 1.
[38] L.L. Ames, Phys. Rev. C 25 (1982) 729.